Proceedings of GT2007
ASME Turbo Expo 2007: Power for Land, Sea and Air
May 14-17, 2007, Montreal, Canada

GT2007-27725

THE BEHAVIOR OF TIP CLEARANCE FLOW AT NEAR-STALL CONDITION IN A TRANSONIC AXIAL COMPRESSOR ROTOR

K. Yamada, K. Funazaki
Department of Mechanical Engineering
Iwate University
Morioka, 020-8551, Japan

M. Furukawa
Department of Mechanical Engineering Science
Kyushu University
Fukuoka, 812-8581, Japan

ABSTRACT

It is known that the tip clearance flow is dominant and very important flow phenomena in axial compressor aerodynamics because the tip clearance flow has a great influence on the stability as well as aerodynamic loss of compressors. Our goal is to clarify the behavior of tip clearance flow at near-stall condition in a transonic axial compressor rotor (NASA Rotor 37). In the present work, steady and unsteady RANS simulations were performed to investigate vortical flow structures and separated flow field near the tip for several different clearance cases. Boundary layer separation on the casing wall and blade suction surface was investigated in detail for near-stall and stall condition. In order to understand such complicated flow field, vortex cores were identified using the critical point theory and a topology of the three-dimensional separated and vortical flows was analyzed. In the nominal clearance case, the breakdown of tip leakage vortex has occurred at a near-stall operating condition because of the interaction of the vortex with the shock wave, leading to a large blockage and unsteadiness in the rotor tip. On the other hand, the calculation with no clearance suggested that the separation on the suction surface was different from that with the nominal clearance. Since the shock wave induced the boundary layer separation on the blade suction surface in the transonic axial compressor rotor, focal-type critical points appeared on the suction surface near the tip at near-stall condition.

INTRODUCTION

The tip clearance flow is strongly related to the aerodynamic performance in compressors and has attracted a great deal of interest. The shear layer is formed between the tip clearance flow and main flow, and rolls up inside the rotor passage to yield a large-scale streamwise slender vortex, a so-called tip leakage vortex. In transonic compressor rotors, the tip leakage vortex interacts with the endwall boundary layer and the shock wave in the passage, which forms the complicated flow field near the tip region. It is difficult to clarify these flow phenomena only by experimental techniques because such phenomena occur in the very small region near the tip in the rotor passage. Therefore, there remain a lot of unclear flow phenomena in transonic compressors.

A number of numerical studies have been performed to investigate the tip clearance flow field in transonic compressor rotors [1–4]. Effects of the tip clearances on a performance in a transonic compressor rotor were investigated by Adamczyk et al. [5]. They indicated that the low-energy fluid appears along the casing due to the interaction of the tip clearance vortex and the rotor passage shock, and showed that an increased flow range was achieved without the tip clearance due to the absence of the vortex/shock interaction. Suder and Celestina [6] reports that the interaction between the tip leakage vortex and the rotor passage shock generates a larger region of high blockage near the tip in the passage as the rotor loadings is increased. In addition, it was indicated that the blockage effect due to the vortex/shock interaction leads to high incidence angles at the tip, which may play a role in bringing about tip stall of the rotor. However, in spite of a number of such efforts details of the blockage in the tip region of transonic compressor rotor have not been revealed yet. In terms of unsteady phenomena of the tip clearance flow, in low-speed axial compressors, the role of the tip clearance flow, such as the

anomalous behavior of the tip leakage vortex at near-stall condition and the relation between the tip leakage vortex and the rotating stall, has been revealed [7–9]. In a transonic axial compressor rotor, the unsteady flow field at stall inception was investigated by the numerical simulation [10], but the origin of the unsteadiness in the rotor passage and details of the unsteady behavior of the tip leakage vortex is not unclear.

The purpose of the present work is to elucidate the tip clearance flow field in a transonic axial compressor rotor, especially at near-stall condition, and to investigate the effect of the tip leakage vortex on a near-stall flow. The tip clearance flow fields in the transonic axial compressor rotor have been investigated by unsteady RANS simulations and by a method of identifying vortex structures based on the critical-point theory. The simulations were executed for three clearance cases, which are the zero, the half, and the nominal clearance case. The zero clearance can get rid of the effect of the tip clearance flow and its result helps us understand it.

TRANSONIC COMPRESSOR ROTOR

A transonic axial compressor rotor, NASA Rotor 37, was used in the present work. The rotor was originally designed as an inlet rotor for a core compressor and tested at NASA Lewis Research Center in the late 1970's. The specification of the rotor is summarized in Table 1. The rotor design pressure ratio is 2.106 at a mass flow of 20.19kg/s. The inlet relative Mach number is 1.13 at the hub and 1.48 at the tip at the design speed of 454m/s (17,188.7rpm). The rotor has 36 blades with a hub-tip ratio of 0.7, an aspect ratio of 1.19, and a tip solidity of 1.288. The tip clearance is 0.356mm. Details of the rotor aerodynamic design were reported by Reid and Moore [11]. Figure 1 shows the location measured using pneumatic probes and laser anemometer system, where radial distributions of static and total pressure, and total temperature, and velocity distributions at some blade-to-blade planes were obtained. This rotor was used for the ASME code assessment 'blind test case' at the ASME/IGTI 39th International Gas Turbine Conference [12]. The simulations were compared to these experimental data [2, 6, 13, 14]. In this study, two other clearances are investigated as well as the nominal clearance (NC). These are the half clearance (HC) and the zero clearance (ZC).

Table 1. Design specification of test compressor

Blade number	36
Radius of tip at leading edge	252mm
Aspect ratio	1.19
Solidity at tip	1.288
Tip clearance	0.356mm (0.45% span)
Hub-tip ratio	0.7
at design	
Tip speed	454m/s (17,188.7rpm)
Total pressure ratio	2.106
Massflow	20.19kg/s
Choke massflow	20.93kg/s

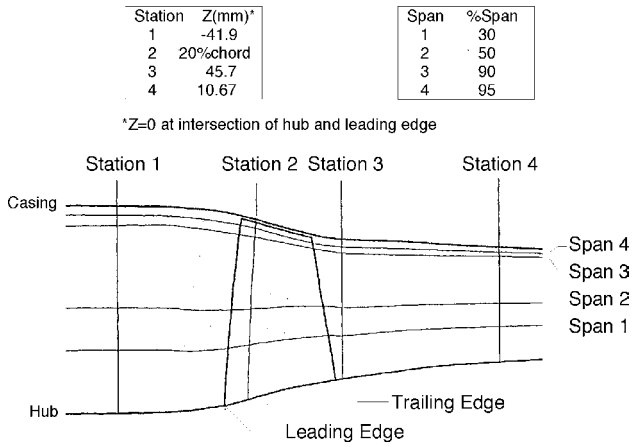

Figure 1. Measurement locations in experiment

NUMERICAL ANALYSIS METHOD

Numerical scheme

The simulations were performed by solving the compressible Navier-Stokes equations using an unfactored implicit upwind relaxation scheme with inner iterations [15, 16]. The numerical method used in the present flow solver is outlined in the following. The three-dimensional Reynolds-averaged Navier-Stokes equations were discretized in space using a cell-centered finite volume formulation and in time using the Euler implicit method. The inviscid fluxes were evaluated by the simple high-resolution upwind scheme (SHUS) [17], which was extended to third-order accurate by the MUSCL interpolation with the Van Albada limiter [18]. The viscous fluxes were determined in a central differencing manner with Gauss's theorem. As for turbulence model, the k-ω turbulence model [19] was employed to estimate the eddy viscosity. A point Gauss-Seidel relaxation method using no approximate factorization was used in time integration [15, 20]. The steady-state computation used the local time step approach to accelerate convergence, where the local time step was given by the CFL number of 5.0. To obtain a time-accurate solution in the unsteady flow simulations, inner iterations, so-called Newton iterations, were introduced at each time step according to Chakravarthy [21]. The scheme achieved up to second-order accurate in time by applying the three-point-backward difference approximation to the temporal derivative [16]. In the present work, nine inner iterations were performed at each time step, and a nondimensional time step size normalized by the rotor tip radius and the inlet sound speed was set to 0.0001. More than 1,300 time steps were included in the

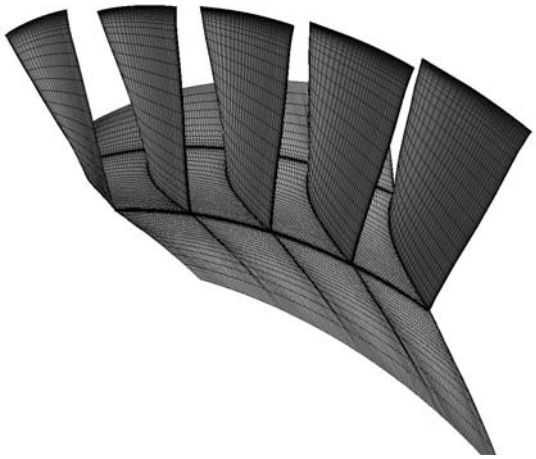

Figure 2. Computational grid (every two lines)

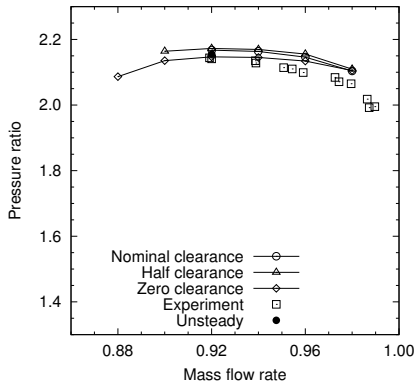

Figure 3. Total pressure ratio characteristics of rotor

period taken for a rotor blade to pass through one pitch. As for boundary condition, fictitious cells were introduced just outside all the boundaries to deal with each boundary condition. The experimental data measured at Station 1 (shown in Fig.1) was used for the inflow boundary. For the outflow boundary, the magnitude of the velocity at the fictitious cells was scaled so as to maintain the imposed total mass flow rate. The single-passage simulations were carried out by applying the periodic boundary condition.

Computational grid

The computational grid is shown in Fig. 2. The composite-grid system was employed to the present simulation. A computational domain was divided into two zones. One zone was a main flow region outside the blade tip clearance, and the other was the tip clearance region. A structured H-type grid was generated in the main flow region, while in the tip clearance region a structured O-type grid was generated. The main grid consisted of 160 cells in the streamwise direction (83 cells on the blade), 105 cells in the spanwise direction, and 78 cells in the pitchwise direction. In order to capture the tip leakage flow field accurately, the grid resolution near the rotor tip was kept high. The grid embedded in the blade tip clearance consisted of $83 \times 20 \times 32$ cells in the chordwise, spanwise and pitchwise directions, respectively. The whole grid system had 1,363,520 cells. The ratio of the minimum grid spacing on solid walls to the blade tip chord length was less than 1.0×10^{-5} to evaluate the viscous fluxes at the walls by applying the no-slip and adiabatic conditions with no wall function method. This minimum grid spacing gave $y^+ < 1$ at the walls.

Visualization Method

The identification of vortex is very useful in understanding the complicated flow fields in turbomachinery. It is hard to have a clear grasp of such complicated flow field by conventional flow visualization techniques such as particle traces, contour plots, secondary vector plots and so on. Therefore, it is critical to identify the vortex structure for the purpose of revealing details of the tip clearance flow field in the transonic axial compressor rotor.

A trajectory of the vortex core is identified by a semi-analytic method developed by Sawada [22]. In his method, assuming that a local velocity field can be linearly parameterized in a tetrahedral computational cell, streamline equations become integrable analytically for the cell, and as a result the obtained streamline expression provides a possible vortex centerline in the cell. In the present study, each hexahedral computational cell is divided into five tetrahedrons to apply Sawada's method. The computational cell crossed by the vortex center line is then regarded as a fraction of the vortex core. The value of unity is given at each vertex of the cells crossed by the vortex center, and zero at the vertices of the other cells. An iso-surface of the specified value is drawn to represent the whole vortex core structure.

RESULTS AND DISCUSSION

Validity of Numerical Simulation

The total pressure ratio characteristics are shown in Fig. 3. All computed results are steady-state simulations. We consider a stall point as a "solution limit" of the steady-state simulation, which is the limit that the simulation cannot converge to a steady-state solution. In each clearance case, the mass flow rate was gradually decreased from the near-peak efficiency point until the stall point, i.e. the solution limit. Almost 91.9% mass flow rate is referred to as stall point in the experiment. In the simulations, the stall mass flow rate turned out to be 88% in the zero and the half clearance case, and 90% in the nominal clearance case, respectively. Therefore, the near-stall condition is referred to here as 90% mass flow rate for the zero and the half clearance cases, and 92% mass flow rate for the nominal clearance case. As far

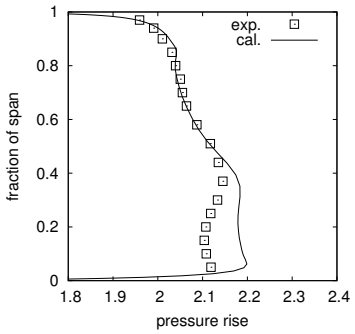

(a) Near-peak efficiency condition

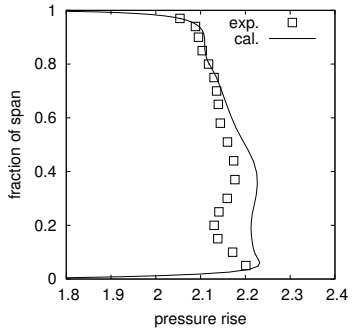

(b) Near-stall condition

Figure 4. Spanwise distributions of total pressure ratio

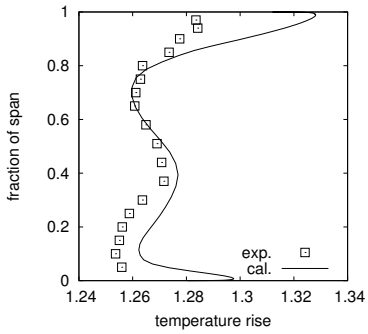

(a) Near-peak efficiency condition

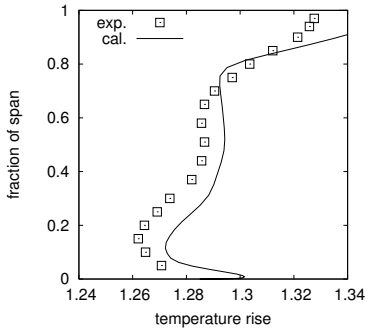

(b) Near-stall condition

Figure 5. Spanwise distributions of total temperature ratio

as the zero clearance case goes, the value at the stall point is additionally shown in the figure for reference. In all of the numerical results, the predictions give a little higher total pressure ratio compared to the experimental ones. For no reason, the zero clearance simulations find a little lower value at each flow condition than the other two clearance cases.

In order to demonstrate validity of the numerical simulations performed in the present work, several comparisons between the numerical and the experimental result are made in terms of the flow fields at two operating points, near-peak efficiency condition (98% mass flow rate) and near-stall condition (92.5% mass flow rate). All the simulation results compared here are from the nominal clearance case. The spanwise distributions of the total pressure ratio and the total temperature ratio are compared in Figs. 4 and 5. The computed pressure ratio and temperature ratio are a little higher than the experimental ones from the hub to the midspan although they qualitatively agree with the experiments. Especially, as shown in Fig. 4, the simulations are unable to predict a "dint" around the hub in the total pressure profiles. It probably seems to be attributed to relatively coarser grid resolution around the hub and the midspan compared to that near the rotor tip althogh some researchers pointed out the effect of the hub leakage flow on the rotor [23]. The prediction was improved in the case of the finer grid. This disagreement leads to a little high total pressure ratio of the simulations as seen in Fig. 3. However, the simulation result has a good agreement with the experimental one near the tip region. It is considered quite good for analyzing the tip clearance flow field in the rotor.

Figures 6 and 7 show the axial velocity distributions at Station 2, which is the plane of 20% chord from the leading edge perpendicular to the axis as shown in Fig. 1. These figures present the limited region only near the casing. In Fig. 6, it is found that the shock wave appears near the midpitch across this plane and the low-energy fluid accumulates just near the casing on the pressure side of the shock wave. It is also confirmed in the experiment. At near-stall condition, the accumulation of the low-energy fluid near the casing becomes much larger than that at near-peak efficiency condition in both of the experiment and the calculation, as shown in Fig. 7. It turns out that the present simulations can exactly predict flow phenomena in the rotor tip region.

Change in Tip Clearance Flow Field with Flow Rate

Figures 8 and 9 show the relative Mach number contour at 95% span. In the Figures, the experimental results measured by laser anemometer are presented for comparison. In the pictures of the calculation results, the relative Mach number contour is colored by white with 0.5 interval and vortex cores in the rotor are also displayed. It is helpful for understanding of the relation

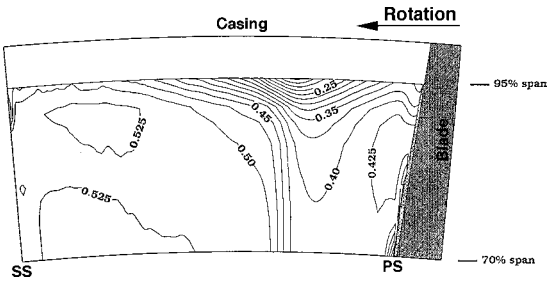

(a) Experiment

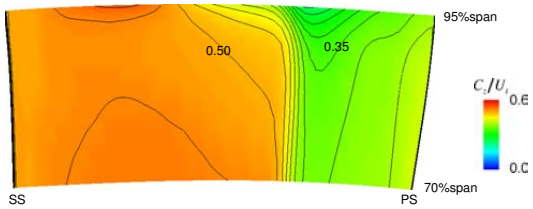

(b) Calculation

Figure 6. Axial velocity distributions at Station 2 at near-peak efficiency condition

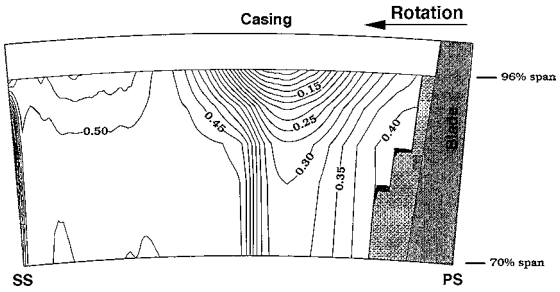

(a) Experiment

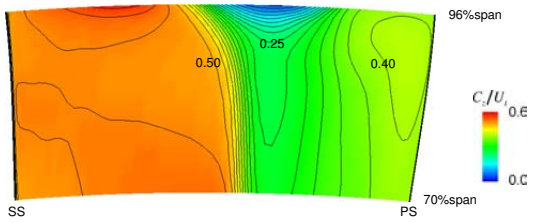

(b) Calculation

Figure 7. Axial velocity distributions at Station 2 at near-stall condition

between the flow field near the rotor tip and the Mach number contour. Vortex cores were identified according to the method above-mentioned and colored with the normalized helicity H_n defined as follows:

$$H_n = \frac{\vec{\xi} \cdot \vec{w}}{|\vec{\xi}||\vec{w}|} \tag{1}$$

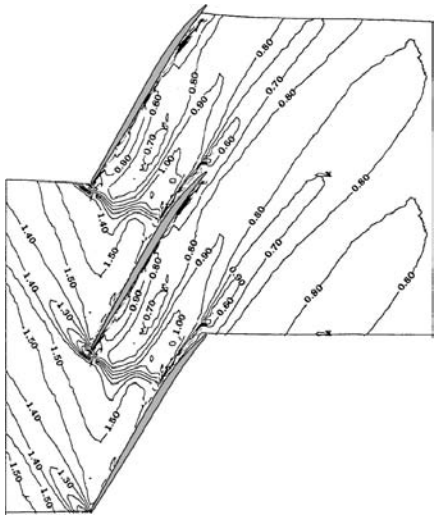

(a) Experiment

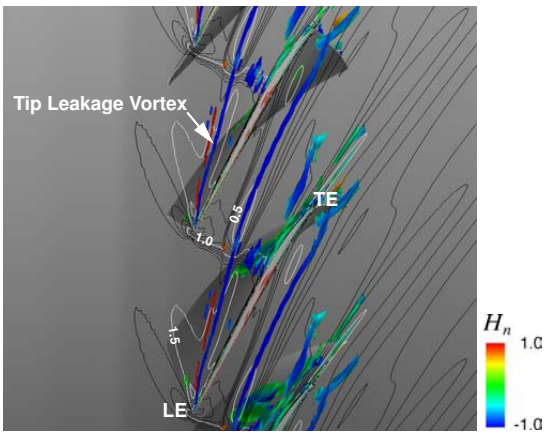

(b) Calculation

Figure 8. Relative Mach number contour of 95% span at near-peak efficiency condition. (b) vortex cores colored with normalized helicity additionally shown

where $\vec{\xi}$ and $\vec{w}$ denote vectors of the absolute vorticity and the relative flow velocity, respectively. The magnitude of the normalized helicity H_n takes the value of unity anywhere the streamwise vortex is present and it can assess the nature of vortex quantitatively, even when the vorticity decays. As seen in the relative Mach number contours from the experiment, there is the shock wave near the leading edge of the rotor blade. The shock wave interacts with the suction surface of the neighboring blade. As shown in Figs. 6 and 7, a low-energy fluid appears just downstream of the shock wave in middle passages. At the near-stall condition, the region of the low-energy fluid dramatically expands and the shock wave is bent in the rotor passage in comparison with the near-peak efficiency condition. The simulations are able to predict such flow phenomena.

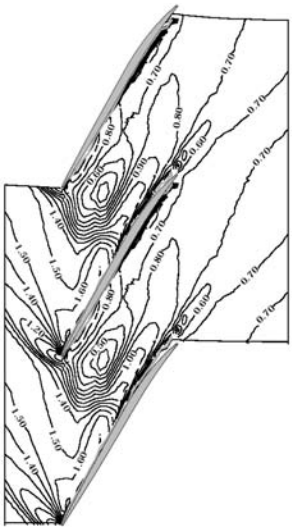

(a) Experiment

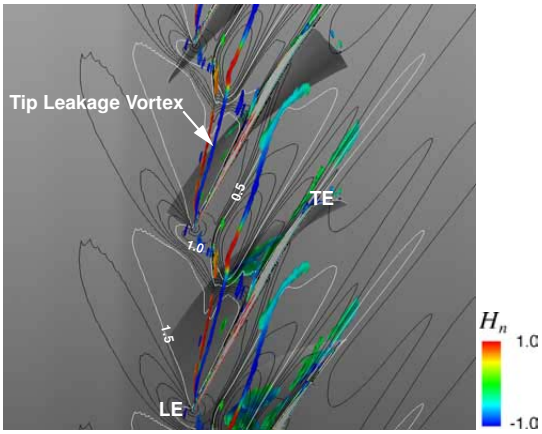

(b) Calculation

Figure 9. Relative Mach number contour of 95% span at near-stall condition. (b) vortex cores colored with normalized helicity additionally shown

In Fig. 8(b), a vortex core is observed in the rotor passage, which lies near the tip from the leading edge of the rotor blade to the pressure side of the adjacent blade. The normalized helicity on that vortex core is almost -1. Since it implies the presence of streamwise vortex, the vortex core is believed to represent the tip leakage vortex rolling up from the leading edge of the rotor tip. It is found that the tip leakage vortex interacts with the shock wave in the rotor passage, and then experiences the abrupt deceleration downstream of the shock wave as will be appreciated from the relative Mach number contour. This leads to expansion of the tip leakage vortex, and finally yielding decelerated flow region, i.e. the low-energy fluid region, just downstream of the shock wave near the rotor tip. At the near-stall condition, as stated the region of the low-energy fluid has become large, where the normalized helicity on the tip leakage vortex indicates opposite sign

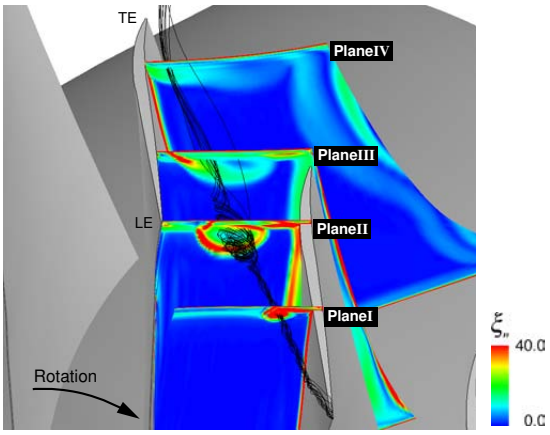

Figure 10. Absolute vorticity distributions on crossflow planes at near-stall condition

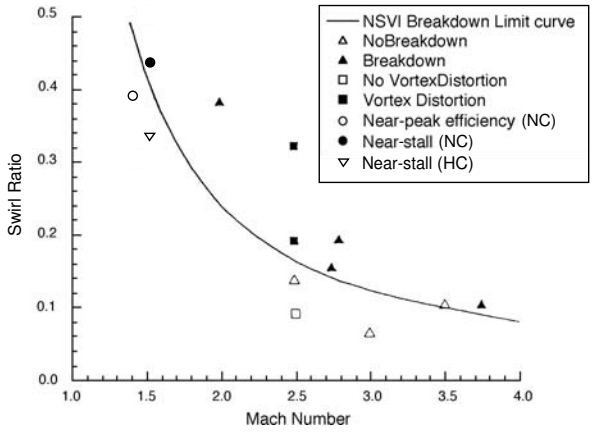

Figure 11. Vortex breakdown limit curve for Normal Shock wave/Vortex Interaction

to the upstream one. Since the sign of the normalized helicity represent direction of swirl relative to the streamwise velocity component at the vortex axis, it implies that reversed flow will be brought about at the center of the tip leakage vortex in the low-energy fluid region. Therefore, it should be said that the tip leakage vortex has experienced significant changes in natures of the streamwise slender vortex. It is expected to relate directly to the large expansion of the low-energy fluid region.

Breakdown of Tip Leakage Vortex at Near-Stall Condition

Shock wave/tip leakage vortex interaction. In Fig. 10, distributions of absolute vorticity coefficient ξ_n in the rotor passage are shown on the clossflow planes nearly perpendicular to the tip leakage vortex. At the same time, the tip leakage streamlines are shown in the figure. The absolute vorticity coef-

ficient ξ_n is defined as follows:

$$\xi_n = \frac{|\vec{\xi}|}{2\omega} \tag{2}$$

where ω is the magnitude of the rotor angular velocity. As seen on the plane I, which is positioned upstream of the shock wave, the tip leakage vortex has a concentrated absolute vorticity before interacting with the shock wave. However, at the plane II, which is located just downstream of the shock wave, the region with high absolute vorticity has expanded abruptly and there is no concentrated absolute vorticity at the center of the tip leakage vortex. As seen in the tip leakage streamlines, the sudden expansion of the tip leakage vortex happens around the plane II downstream of the shock wave, where the recirculation appears around the center of the vortex. These flow phenomena in the tip leakage vortex downstream of the shock wave, i.e. the occurrence of the recirculation (stagnation) region at the vortex center, the unexpected expansion, and the lack of concentrated absolute vorticity in the vortex core, correspond to some features of "vortex breakdown" [24, 25]. The vortex breakdown has some features such as a reversed flow region, a sudden expansion of the vortex, and large-scale flow fluctuations. It is well known that the vortex breakdown occurs in leading edge vortices over delta wings, swirling jets in combustion chambers, and swirling flows in draft tubes of hydraulic turbines. Recently, it has been observed even in turbomachineries: a low-speed axial compressor rotor [7] and a transonic compressor rotor [26, 27]. The vortex breakdown brings about an abrupt change in the vortex core structure, but its stability criterion is not fully elucidated yet. It has been found, however, that there are two types in the vortex breakdown: bubble type and spiral type, and appearance of the vortex breakdown can be influenced by an adverse pressure gradient in streamwise direction and the swirl intensity of the vortex. It is easy to imagine that the vortex breakdown can be caused by the shock wave/vortex interaction. As the mass flow rate is reduced, the swirl intensity of the tip leakage vortex increases with the blade loading. It finally gives rise to the breakdown of the tip leakage vortex at near-stall condition. In this way, in the present transonic axial compressor rotor the breakdown of the tip leakage vortex is considered to have happened because of the interaction with the shock wave at the near-stall condition, judging the flow phenomena in a comprehensive manner. It should be said that the tip leakage vortex breakdown at the near-stall condition yields the large expansion of the low-energy fluid region shown in Fig. 9, and leads to the large blockage effect near the tip in the rotor passage.

The criteria of the vortex breakdown in the case of NSVI (Normal Shock wave/Vortex Interaction) was analytically investigated by Smart et al. [28]. Figure 11 shows the breakdown limit curve for NSVI, which is introduced by them, and the present simulation results of the tip leakage vortex/shock wave interaction in the transonic compressor rotor. The curve shown in the figure analytically predicts the presence of the breakdown of a streamwise slender vortex caused by the interaction with the normal shock wave, and is presented with respect to the freestream Mach number and the swirl ratio τ upstream of the shock wave. The swirl ratio τ is defined as follows:

$$\tau = \frac{\Gamma}{2\pi r_{core} V_a} = \frac{\Lambda_{max}}{V_a} \tag{3}$$

where Γ is the circulation of the vortex, r_{core} is the radius of the vortex core, Λ_{max} is the maximum of swirl velocity component in the vortex core, and V_a is the velocity component along the vortex axis direction at the vortex axis. The larger circulation and the smaller core radius the vortex has, the higher the swirl ratio becomes. In the present work, the swirl ratio was estimated from Λ_{max} due to the difficulty in calculating the circulation of the tip leakage vortex. The upper side from the curve corresponds with the vortex breakdown region. The symbols are marked out with black in the case that the vortex breakdown occurs. The present numerical simulations represent a good correlation with the NSVI breakdown limit as well as a number of shock/vortex interaction experiments. The simulation result at the near-stall condition is close to the curve, which means that just before the stall point the breakdown of the tip leakage vortex has occurred. On the other hand, in the half clearance case (HC), there is no breakdown of the tip leakage vortex even at the near-stall condition. As mentioned, the near-stall condition for the half clearance case is defined here as 90% mass flow rate.

Figure 13 shows the relative Mach number contour at 95% span and the vortical flow structures for the half clearance at the near-stall condition. For comparison, the result for the nominal clearance at 94% mass flow rate, which is slightly larger than the near-stall condition, is shown in Fig. 12. The tip clearance flow field at the near-stall condition for the half clearance closely resembles that before the tip leakage vortex breakdown for the nominal clearance case. In addition, the sign of the normalized helicity on the tip leakage vortex has not changed downstream of the shock wave contrary to the nominal clearance case in Fig. 9. In the half clearance, the swirl intensity of the tip leakage vortex is not still strong enough to cause the vortex breakdown even at the near-stall condition because of the small clearance. The absence of the vortex breakdown in the tip clearance flow field reduces the blockage effect near the tip, which ultimately results in a wide flow range compared to the nominal clearance case.

Shock wave/boundary layer interaction. Figure 14 shows the limiting streamlines on the casing wall for the nominal clearance case. The boundary layer separates from the casing wall because of the shock wave and the tip clearance flow.

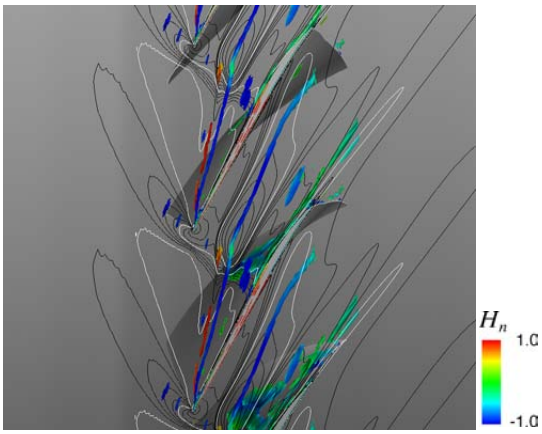

Figure 12. Vortical flow structures and relative Mach number contour near the tip at 94%choke flow condition (NC)

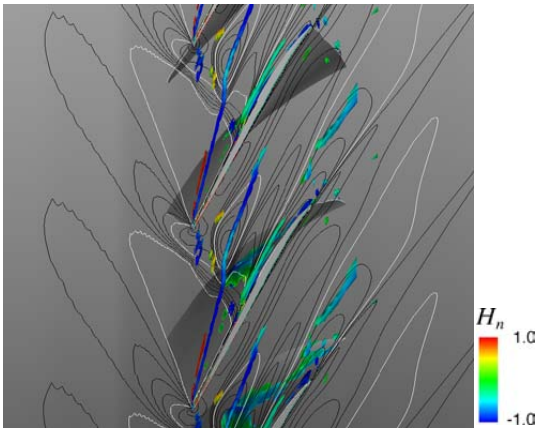

Figure 13. Vortical flow structures and relative Mach number contour near the tip at near-stall condition (HC)

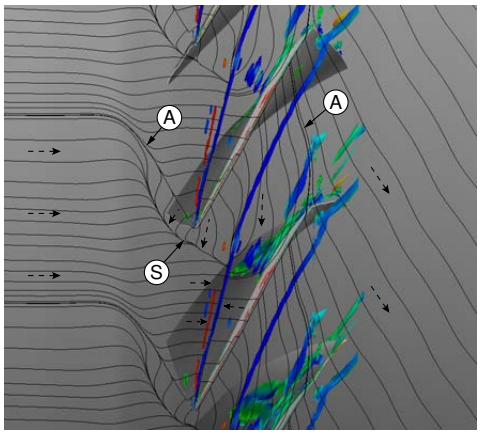

(a) Near-peak efficiency condition

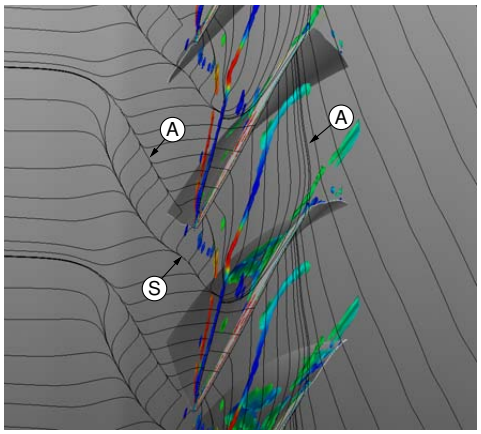

(b) Near-stall condition

Figure 14. Limiting streamlines on the casing wall (NC)

The attachment line of its separated flow on the casing lies at almost the exit of the rotor passage. Therefore, the separation region covers most part of the passage and a strong reversed flow happens at the suction side around the aft part of the passage. That reversed flow is sharply distinguished from the "back flow" mentioned in [29], because it is seen at the near-peak efficiency condition. At the near-stall condition, the shock wave moves upstream compared to the near-peak efficiency condition and the separation region expands with the movement of the shock wave.

Figures 15 and 16 show the limiting streamlines on the blade suction surface. Near the hub, there are the bifurcation lines of separation and attachment around the mid-chord due to the interaction of the shock wave. However, it is different near the rotor tip. As seen in Fig. 15, the shock wave near the rotor tip interacts with the suction surface at the aft part of the blade at the near-peak efficiency condition. On the other hand, at the near-stall condition the shock wave moves upstream with the flow rate decreased as mentioned above and the separation line near the tip due to the interaction of the shock wave is found at almost the same mid-chord as the one near the hub. In the case of the zero clearance at the stall and the near-stall condition, the separation line moves upstream as well as the nominal clearance case at the near-stall condition as shown in Fig. 16. Therefore, the movement of the shock wave seems to have little relevance to the tip leakage vortex breakdown. The near-stall condition and the stall condition in the zero clearance case are different from each other in the topology of the limiting streamlines near the rotor tip. At the stall condition, focal-type critical points (three-dimensional separation and attachment) appear near the rotor tip and the separation line rather closes in upon the leading edge. The focal-type critical point implies that three-dimensional flow field is formed near the rotor tip in contrast to the two-dimensional flow field near the hub. The reversed flow at the trailing edge is enhanced near the rotor tip and another separation line due to this reversed flow reaches the separation line due to the shock wave interac-

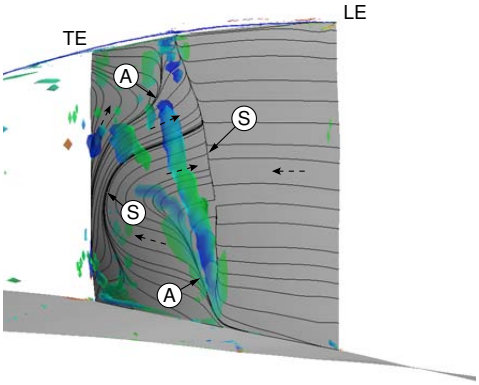

(a) Near-peak efficiency condition

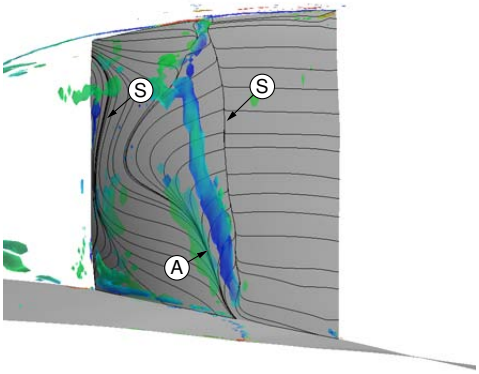

(b) Near-stall condition

Figure 15. Limiting streamlines on the blade suction surface (NC)

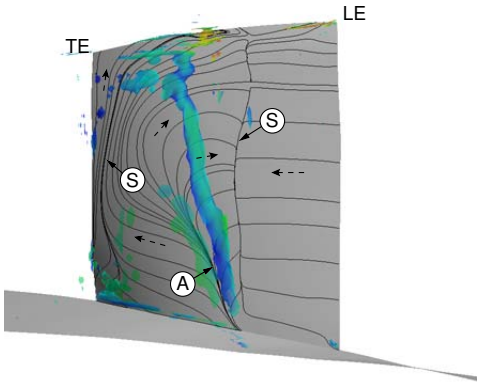

(a) Near-stall condition

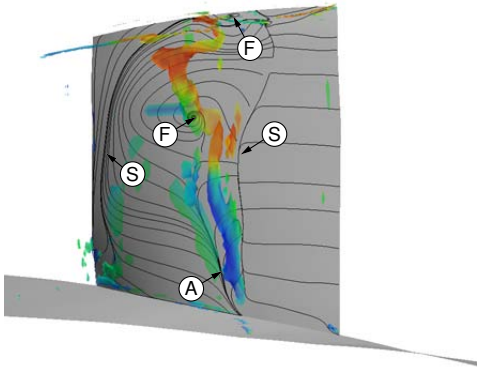

(b) stall condition

Figure 16. Limiting streamlines on the blade suction surface (ZC)

tion near the tip. Therefore, near the tip the separated flow by the shock wave is not re-attached on the suction surface until the trailing edge of the rotor, which produces a large blockage effect. The blockage effects due to the boundary layer separation on the casing wall and the blade suction surface near the tip is expected to lead to the stall of the compressor rotor in the zero clearance case of the present single passage simulation.

Figure 17 illustrates the shock wave/tip leakage vortex interaction in a transonic compressor rotor. Two possible cases are described as weak and strong interaction. The impact of the interaction, which will bring the vortex breakdown, depends on three factors. One is the swirl intensity of the vortex. Another is a pressure difference on upstream and downstream of the shock wave. The other is an angle formed by the vortex and the shock wave in the interaction. The interaction becomes strong as the angle approaches right angle. The emergence of the tip leakage vortex will be explained as follows. As the flow rate is reduced, the shock wave near the tip moves upstream in the compressor rotor. The shock wave makes approximately perpendicular to the tip leakage vortex. In addition, the swirl intensity of the tip leakage vortex increases with the flow rate decreased. The increased impact of the shock wave/tip leakage vortex interaction eventually gives rise to the breakdown of the tip leakage vortex at near-stall condition.

Unsteady Behavior of Tip Leakage Vortex Due to Its Breakdown

The vortex breakdown has a large-scale unsteady nature. It is expected to induce unsteadiness in the tip clearance flow field in the rotor. The unsteady flow behavior due to the breakdown of the tip leakage vortex is discussed in this section. The unsteady simulation was conducted at the near-stall condition for the nominal clearance to investigate the breakdown-induced unsteady flow field near the rotor tip.

Figure 18 shows an instantaneous tip clearance flow field at the near-stall condition obtained by the unsteady simulation for the nominal clearance. In the figure, the relative Mach number contour at 95% span and vortex cores colored with the normal-

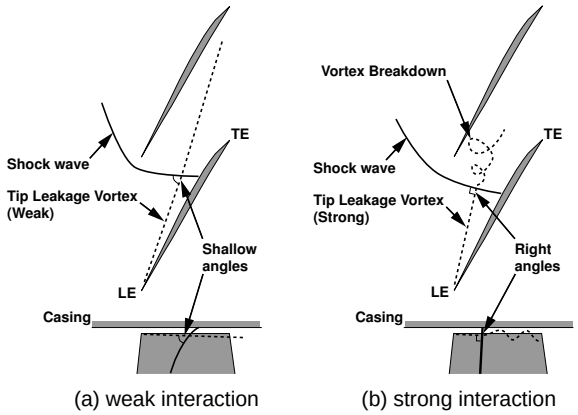

(a) weak interaction (b) strong interaction

Figure 17. Sketch of shock wave/tip leakage vortex interaction

ized helicity are shown as in the case of Fig. 9. Although the form of the tip leakage vortex breakdown is bubble-type in the steady-state simulation as shown in Fig. 9, it has changed to spiral-type because of its unsteadiness. The tip leakage vortex twists and turns in the rotor passage, and violently fluctuates with time while interacting with the pressure surface near the leading edge of the adjacent blade. Since it is followed by the fluctuation of the low-energy fluid due to the tip leakage vortex breakdown at the same time, the shock wave also fluctuates upstream and downstream with this. That unsteady flow phenomena due to the tip leakage vortex breakdown is periodically repeated. The cyclic interaction of the tip leakage vortex with the adjacent blade leads to the fluctuation of the blade torque.

Figure 19 shows the time history of blade torque coefficient C_t, which is defined as follows:

$$C_t = \frac{T}{\rho U_t^2 r_t^2 / 2} \tag{4}$$

where ρ, U_t, r_t and T are the density, the blade tip speed, the blade tip radius, and the blade torque, respectively. The time-frequency analysis has been executed based on the wavelet transform for the time fluctuation data of the blade torque coefficient. The predominant frequency appeared around 66% of the blade passing frequency, which corresponds to 6.8kHz, in the wavelet spectrum except the transitional period of the simulation.

At the near-stall condition, the tip clearance flow still does not spill over into the adjacent blade passage though the tip leakage vortex interacts with the pressure surface near the leading edge of the adjacent blade. At the stall condition, the tip clearance flow must spill over into the adjacent blade passage because the fluctuation of the tip leakage vortex is amplified. In contrast to the stalling process in the low-speed compressor described by Hoying et al. [9], the breakdown of the tip leakage vortex is responsible for the spillage in the present transonic axial compressor rotor. The breakdown of the tip leakage vortex has happened

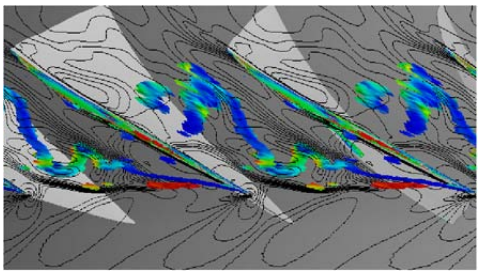

Figure 18. Instantaneous vortical flow structure and relative Mach number contour near the tip at near-stall condition (NC)

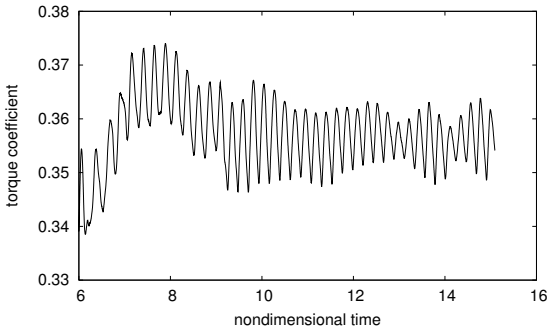

Figure 19. Time history of blade torque at near-stall condition (NC)

before tip leakage vortex trajectory becomes perpendicular to the axial direction, which leads to the stall at larger mass flow rate. It should be noted that the results are from single-passage simulations. The interaction of the tip leakage vortex with the neighboring blade surface may trigger a propagated flow phenomenon like the rotating instability [30, 31]. Actually, in spite of the single-passage calculation the simulation shows features similar to the rotating instability in the frequency and pressure fluctuation at the pressure side near the tip. Since the results of this study are from the single-passage calculation, they might not exactly represent the actual stall mechanism and/or the real flow phenomena at near-stall condition. The present simulations, however, are believed to indicate the possible presence of above flow phenomena at near-stall condition and stall inception in transonic axial compressor rotors. It is necessary to compare the present single-passage simulations with multi-passage simulations and to investigate relations between both two simulation results in the future work.

CONCLUSIONS

The tip clearance flow fields in the transonic axial compressor rotor have been investigated by unsteady RANS simulations and by a method of identifying vortex structures based on the critical-point theory. The results are summarized as follows:

1. In the nominal clearance case, breakdown of the tip leakage vortex occurred downstream of the shock wave at the near-stall condition. It is because the interaction between the tip leakage vortex and the shock wave becomes strong as the flow rate is reduced. The tip leakage vortex breakdown is responsible for the low-energy fluid downstream of the shock wave in the rotor passage, which brings a large blockage effect near the rotor tip.
2. In the zero clearance case, the flow range is extended compared to that in the nominal clearance case owing to absence of the shock wave/tip leakage vortex interaction. In the half clearance case, the breakdown of the tip leakage vortex is not observed because of the weak interaction between the tip leakage vortex and the shock wave. Therefore, the flow range is almost the same as that in the zero clearance case.
3. The breakdown of the tip leakage vortex leads to not only the large blockage effect near the tip but also the unsteady flow phenomena in the rotor passage. The unsteady behavior of the tip leakage vortex due to its breakdown gives rise to the fluctuations of the blade torque, the low-energy fluid and the shock wave near the rotor tip.
4. The large blockage effect and the unsteadiness due to the tip leakage vortex breakdown may be related to the spillage of the tip clearance flow at the stall inception. It is necessary to carry out multi-passage simulations and to investigate relations to the single-passage simulations in the future work.

ACKNOWLEDGMENT

The present research was partially supported by the Ministry of Education, Culture, Sports, Science and Technology, Grant-in-Aid for Scientific Research (A), KAKENHI 16206021, 2006.

REFERENCES

[1] Copenhaver, W. W., Mayhew, E. R., Hah, C., and Wadia, A. R., 1996. "The effect of tip clearance on a swept transonic compressor rotor". *ASME J. Turbomachinery,* **118**, pp. 230–239.

[2] Chima, R. V., 1998. "Calculation of tip clearance effect in a transonic compressor rotor". *ASME J. Turbomachinery,* **120**, pp. 131–140.

[3] Gerolymos, G. A., and Vallet, I., 1999. "Tip-clearance and secondary flows in a transonic compressor rotor". *ASME J. Turbomachinery,* **121**, pp. 751–762.

[4] Hoeger, M., Fritsch, G., and Bauer, D., 1999. "Numerical simulation of the shock-tip leakage vortex interaction in a hpc front stage". *ASME J. Turbomachinery,* **121**, pp. 456–468.

[5] Adamczyk, J. J., Celestina, M. L., and Greitzer, E. M., 1993. "The role of tip clearance in high-speed fan stall". *ASME J. Turbomachinery,* **115**, pp. 28–39.

[6] Suder, K. L., and Celestina, M. L., 1996. "Experiment and computational investigation of the tip clearance flow in a transonic axial compressor rotor". *ASME J. Turbomachinery,* **118**, pp. 218–229.

[7] Furukawa, M., Inoue, M., Saiki, K., and Yamada, K., 1999. "The role of tip leakage vortex breakdown in compressor rotor aerodynamics". *ASME J. Turbomachinery,* **121**(3), pp. 469–480.

[8] Furukawa, M., Saiki, K., Yamada, K., and Inoue, M., 2000. "Unsteady flow behavior due to breakdown of tip leakage vortex in an axial compressor rotor at near-stall condition". ASME. Paper No. 2000-GT-666.

[9] Hoying, D. A., Tan, C. S., Vo, H. D., and Greitzer, E. M., 1999. "Role of blade passage flow structures in axial compressor rotating stall inception". *ASME J. Turbomachinery,* **121**, pp. 735–742.

[10] Hah, C., Bergner, J., and Schiffer, H., 2006. "Short length-scale rotating stall inception in a transonic axial compressor - criteria and mechanisms". ASME. GT2006-90045.

[11] Reid, L., and Moore, R. D., 1978. "Design and overall performance of four highly-loaded, high-speed inlet stages for an advanced, high-pressure-ratio core compressor". NASA. TP-1337.

[12] Strazisar, A. J., and Denton, J. D., 1995. "Cfd code assessment in turbomachinery - a progress report". In IGTI Global Gas Turbine News, pp. 12–14.

[13] Hah, C., and Loellbach, J., 1999. "Development of hub corner stall and its influence on the performance of axial compressor blade rows". *ASME J. Turbomachinery,* **121**, pp. 67–77.

[14] Suder, K. L., 1998. "Blockage development in a transonic, axial compressor rotor". *ASME J. Turbomachinery,* **120**(3), pp. 465–476.

[15] Furukawa, M., Nakano, T., and Inoue, M., 1992. "Unsteady navier-stokes simulation of transonic cascade flow using an unfactored implicit upwind relaxation scheme with inner iterations". *ASME J. Turbomachinery,* **114**(3), pp. 599–606.

[16] Inoue, M., and Furukawa, M., 1994. "Artificial dissipative and upwind schemes for turbomachinery blade flow calculation". VKI Lecture Series. No. 1994-06.

[17] Shima, E., and Jounouchi, T., 1997. "Role of cfd in aeronautical engineering (no.14)-ausm type upwind schemes". In the 14th NAL Symposium on Aircraft Computational Aerodynamics, National Aerospace Lab., pp. 7–12. NAL SP-34.

[18] Anderson, W. K., Thomas, J. L., and van Leer, B., 1986. "Comparison of finite volume flux vector splittings for the euler equations". *AIAA Journal,* **24**(9), pp. 1453–1460.

[19] Wilcox, D. C., 1994. "Simulation of transition with a two-equation turbulence model". *AIAA Journal,* **32**(2), pp. 247–255.

[20] Furukawa, M., Saiki, K., and Inoue, M., 1995. "Numerical

simulation of three-dimensional viscous flow in diagonal flow impeller". In Numerical Simulations in Turbomachinery, ASME FED, Vol. 227, pp. 22–39.
[21] Chakravarthy, S. R., 1984. "Relaxation method for unfactored implicit upwind schemes". AIAA. Paper No. 84-0165.
[22] Sawada, K., 1995. "A convenient visualization method for identifying vortex centers". *Japan Soc. of Aero. Space Sci.,* **38**(120), pp. 102–116.
[23] Shabbir, A., Celestina, M., Adamczyk, J., and Strazisar, A., 1997. "The effect of hub leakage flow on two high speed axial flow compressor rotors". ASME. Paper No. 97-GT-346.
[24] Leibovich, S., 1978. "The structure of vortex breakdown". *Annual Review of Fluid Mechanics,* **10**, pp. 221–246.
[25] Deley, J. M., 1994. "Aspects of vortex breakdown". *Prog. Aerospace Sci.,* **30**, pp. 1–59.
[26] Schlechtriem, S., and Lotzerich, M., 1997. "Breakdown of tip leakage vortices in compressors at flow conditions close to stall". ASME. Paper No. 97-GT-41.
[27] Yamada, K., Furukawa, M., Nakano, T., Inoue, M., and Funazaki, K., 2004. "Unsteady three-dimensional flow phenomena due to breakdown of tip leakage vortex in a transonic axial compressor rotor". In ASME. GT2004-53745.
[28] Smart, M. K., and Kalkhoran, I. M., 1997. "Flow model for predicting normal shock wave induced vortex breakdown". *AIAA Journal,* **35**(10), pp. 1589–1596.
[29] Vo, H. D., Tan, C. S., and Greitzer, E. M., 2005. "Criteria for spike initiated rotating stall". ASME. GT2005-68374.
[30] Mailach, R., Lehmann, I., and Vogeler, K., 2001. "Rotating instabilities in an axial compressor originating from the fluctuating blade tip vortex". *ASME J. Turbomachinery,* **123**, pp. 453–463.
[31] März, J., Hah, C., and Neise, W., 2002. "An experimental and numerical investigation into the mechanisms of rotating instability". *ASME J. Turbomachinery,* **124**, pp. 367–375.